Research Square

Preprints are preliminary reports that have not undergone peer review. They should not be considered conclusive, used to inform clinical practice, or referenced by the media as validated information.

Ultrasound-Intensified Solvent-Free Lipase-Catalyzed Synthesis of 2-Phenethyl Octanoate: Molecular Docking and ANN-Based Process Optimization

Ming-Fang Tsai
National Chung Hsing University
Shuo-Wen Tsai
National Chung Hsing University
Chwen-Jen Shieh
cjshieh@nchu.edu.tw

National Chung Hsing University

Research Article

Keywords: Artificial neural network, Green metrics, Molecular docking, 2-Phenethyl octanoate, Solvent-free biocatalysis, Ultrasound process intensification

Posted Date: October 15th, 2026

DOI: https://doi.org/10.21203/rs.3.rs-11207996/v1

License: This work is licensed under a Creative Commons Attribution 4.0 International License. Read Full License

Additional Declarations: No competing interests reported.

Ultrasound-Intensified Solvent-Free Lipase-Catalyzed Synthesis of 2-Phenethyl Octanoate: Molecular Docking and ANN-Based Process Optimization

Ming-Fang Tsai[1,2], Shuo-Wen Tsai[1]*, Chwen-Jen Shieh[2]*

[1]*Department of Food Science and Biotechnology, National Chung Hsing University, Taichung 40227, Taiwan*

[2]*Biotechnology Center, National Chung Hsing University, 250 Kuokuang Road, Taichung 40227, Taiwan*

*Authors to whom correspondence should be addressed. E-mail: tsaishuowen@nchu.edu.tw (S.-W. Tsai); cjshieh@nchu.edu.tw (C.-J. Shieh)

Keywords:

Artificial neural network; Green metrics; Molecular docking; 2-Phenethyl octanoate; Solvent-free biocatalysis; Ultrasound process intensification

Abstract

2-Phenethyl octanoate (2-PO) is a food flavoring ester with a mild fruity, wine-like odor. This paper introduces an ultrasound-intensified solvent-free lipase-catalyzed process for 2-PO synthesis from 2-phenylethanol and octanoic acid using Novozym® 435. Under ANN-optimized conditions, the process achieved 87.01% molar conversion within 6.48 min, versus 45.84 ± 2.66% without ultrasound, confirming its benefit in the solvent-free system. ANN modeling (R^2 = 0.9974, RMSE = 0.5535) outperformed response surface methodology (RSM; R^2 = 0.9333, RMSE = 4.1984) in capturing nonlinear variable interactions, with a predicted optimum of 88.16% validated experimentally as 87.01 ± 1.02%. Docking analysis supported substrate positioning within the Ser105–His224–Asp187 catalytic triad, while the stronger predicted binding affinity of 2-PO (−6.524 kcal/mol) may explain the product-associated active-site occupancy and kinetic plateau observed. Green metrics confirmed process sustainability, with an E-factor of 0.49 kg/kg and atom economy of 93.24%, reflecting minimal waste in the solvent-free system. After 10 cycles, Novozym® 435 retained 88.8% of its initial molar conversion, indicating operational stability. These findings establish a docking-guided, ultrasound-assisted framework for the scalable, sustainable biosynthesis of food-grade aromatic esters for natural flavor applications.

Introduction

2-Phenethyl octanoate (2-PO) is a naturally occurring volatile ester with a fruity, wine-like aroma, found in okra seeds and alcoholic beverages (Camciuc et al., 1998), and recognized as a safe flavoring agent by the Joint FAO/WHO Expert Committee on Food Additives (JECFA) (Joint FAO/WHO Expert Committee on Food Additives, 2002). Its aromatic alcohol substrate, 2-phenylethanol (2-PE), is a commercially significant fragrance predominantly synthesized via petrochemical routes, with over 90% of the current supply relying on such processes; although microbial fermentation offers a bio-based alternative, 2-PE exhibits cytotoxicity toward producing microorganisms at concentrations of 2 to 4 g/L, severely restricting fermentation titers (Bernardino et al., 2024). To reduce dependence on petrochemical-derived precursors and meet growing demands for clean-label ingredients, lipase-catalyzed esterification of 2-PE with octanoic acid (C8) in a solvent-free system represents an effective synthesis strategy. However, documented enzymatic routes to 2-PO remain limited, and reported processes have relied on toxic organic solvents such as hexane (Šinkūnienė et al., 2014). Transitioning to a solvent-free biocatalytic system eliminates hazardous solvent waste, increases yields, and simplifies downstream purification (Sousa et al., 2021). This strategy aligns with the modernized principles of green chemistry prioritizing solvent elimination (Lipshutz & Handa, 2026), providing a viable pathway toward sustainable, clean-label flavor ingredient production.

Novozym® 435, an immobilized lipase B from Candida antarctica (CALB), was selected as the biocatalyst for its broad substrate specificity toward alcohol substrates and proven efficacy in the esterification of C8 with various alcohols (Gandhi & Mukherjee, 2001). In esterification strategies, direct esterification in a solvent-free system maximizes process sustainability. However, the complete elimination of auxiliary solvents imposes substantial mass-transfer limitations within the neat reaction medium, while the accumulation of by-product water within the macroporous support promotes partial dissociation of unreacted C8, lowering the local pH and potentially inducing irreversible enzyme inactivation (Sousa et al., 2021). Consequently, in the solvent-free synthesis of C8 acyl donor-based esters such as octyl caprylate, achieving high conversion still required 3 h to reach 94.5% conversion (Sousa et al., 2020). Beyond these macroscopic mass-transfer and stability challenges, the inherent catalytic feasibility is fundamentally dictated by substrate-enzyme interactions at the active site. These considerations prompted the implementation of molecular docking analysis prior to experimental assays, examining whether the CALB active site can accommodate the sterically demanding 2-PE alongside C8 under induced-fit conditions (Juhl et al., 2009).

In addition to viscosity-related constraints, the steric demands of 2-PE further restrict catalytic efficiency within the CALB active site. The active site of CALB is located at the base of a narrow hydrophobic channel, where the phenyl ring of 2-PE imposes significant

steric hindrance, representing a catalytic bottleneck that cannot be resolved through process optimization alone. As the steric hindrance of the secondary or aromatic group on a substrate increases, the relative activity of CALB can decline markedly (up to 1000-fold for highly hindered alcohols) due to spatial conflicts within the active site (Cha et al., 2019; Kuo et al., 2025). Despite steric restriction imposed by Trp104, a nucleophilic attack distance (O⋯C) of 3.5 Å was observed, consistent with a putative near-attack conformation (NAC) (Hur & Bruice, 2003). The esterification of aromatic alcohols therefore typically requires prolonged reaction times; for example, synthesis of eugenol esters, which are structurally similar to 2-PE, required 4–6 hours and elevated substrate molar ratios to attain high yields, even when organic solvents were employed (Chaibakhsh et al., 2012; Horchani et al., 2010; Mat Radzi et al., 2016). Similarly, esterification of cinnamic acid, where the aromatic moiety resides on the acid substrate, requires organic co-solvents for viable mass transfer, precluding a solvent-free approach (Suarez-Escobedo & Gotor-Fernandez, 2021). The concurrent use of 2-PE and high-viscosity C8 therefore imposes a "dual mass transfer limitation": the high viscosity hinders bulk-phase diffusion (Sousa et al., 2021), while the steric bulk of 2-PE restricts substrate accessibility to the active site. These structural constraints and the risk of acid-induced enzyme inactivation (Sousa et al., 2021) make molecular docking an essential prerequisite for validating system feasibility prior to experimental implementation.

With the structural compatibility and thermodynamic feasibility of the CALB/2-PE/C8 system supported by the docking analysis within the Ser105–His224–Asp187 catalytic triad, ultrasonication was subsequently integrated as a green process intensification strategy. Acoustic cavitation collapses micro-bubbles under extreme local heat and pressure, disrupting phase boundaries between substrates, enhancing mass transfer, and lowering the activation energy barrier for enzymatic esterification (Huang, Li, et al., 2017; Xu et al., 2018). Building on our group's prior work on ultrasound-assisted synthesis of value-added esters (Kuo et al., 2013), and informed by successful precedents in solvent-free xylityl acyl ester production (Nieto et al., 2021), the present study thus provides a mechanistically informed basis for linking substrate-level molecular recognition to the rational design of solvent-free biocatalytic processes.

Therefore, this study aimed to develop a solvent-free biocatalytic process for 2-PO synthesis by coupling molecular docking simulations with ultrasound-assisted process intensification. Molecular docking was first performed to evaluate substrate accommodation and binding behavior of 2-PE and C8 within the CALB catalytic cleft, guiding the subsequent experimental design. A central composite rotatable design (CCRD), response surface methodology (RSM), and artificial neural networks (ANN) were then integrated to systematically identify the optimal conditions for 2-PO synthesis. The framework established herein offers a transferable, solvent-free biocatalytic route for

96 producing food-grade 2-PO, meeting clean-label demands for sustainable flavor
97 manufacturing in the food industry.

98 **2. Materials and Methods**

99 2.1 *Materials*

100 Immobilized lipase Novozym® 435 (10,000 propyl laurate units (PLU) g^{-1})
101 from *Candida antarctica* B (EC 3.1.1.3) supported on a macroporous acrylic resin was
102 purchased from Novo Nordisk Bioindustrials Inc. (Copenhagen, Denmark). 2-PE was
103 obtained from Alfa Aesar (Haverhill, MA, USA), and C8 from Sigma Chemical Co. (St.
104 Louis, MO, USA). Methanol was obtained from Aencore (Melbourne, Victoria, Australia).
105 Molecular sieves (4 Å) were purchased from Davison Chemical Co. (Baltimore, MD,
106 USA). All chemicals were of analytical reagent grade.

107 2.2 *Ultrasound-Assisted Solvent-Free Synthesis of 2-PO*

108 All reagents were dehydrated with 4 Å molecular sieves for 24 h before use. The reaction
109 mixture was prepared by combining C8 and 2-PE at a fixed molar ratio in a sealed glass
110 tube (total volume 1 mL), with 2-PE serving as both substrate and bulk phase. The reaction
111 was initiated by adding Novozym® 435 (500–1500 PLU). The tube was placed in a
112 temperature-controlled ultrasonic bath (Delta DC150H, Dogger Science, New Taipei,
113 Taiwan) operating at 40 kHz under various conditions of reaction time (2–10 min),

temperature (35–75 °C), and ultrasonic power (90–150 W). The position of the tube within the bath was fixed to ensure constant ultrasonic intensity. At the end of the reaction, the mixture was immediately cooled in an ice bath, and methanol was added to quench enzymatic activity prior to analysis. To evaluate the specific contribution of ultrasonic irradiation, a control reaction was performed under the same ANN-optimized conditions (reaction time 6.48 min, temperature 57.34 °C, enzyme amount 1216.87 PLU) using the identical ultrasonic bath system with temperature control maintained at 57.34 °C, but with the ultrasonic function switched off. All other procedural steps, including reagent preparation, reaction termination, and analysis, were performed as described above.

2.3 *Experimental Design and Optimization by RSM*

A 5-level-4-factor central composite rotatable design (CCRD) was employed to optimize the synthesis conditions. The four independent variables were reaction time (X_1, 2–10 min), temperature (X_2, 35–75 °C), enzyme amount (X_3, 500–1500 PLU), and ultrasonic power (X_4, 90–150 W), as listed in Table 1. The design consisted of 27 experimental runs, including 16 factorial points, 8 axial points, and 3 center points for estimation of pure error. The experimental matrix and corresponding molar conversions are presented in Table 2. The relationship between the independent variables and the response (molar conversion, %) was modeled by a second-order polynomial equation, Eq. (1), using JMP® software (Version 8.0, SAS Institute Inc., Cary, NC, USA).

$$Y = \beta_{\{k0\}} + \sum_{\{i=1\}}^{4} \beta_{\{ki\}X_i} + \sum_{\{i=1\}}^{4} \beta_{\{kii\}X_i^2} + \sum_{\{i=1\}}^{3} \sum_{\{j=i+1\}}^{4} \beta_{\{kij\}X_{iX_j}} \quad \ldots\ldots\ldots(1)$$

2.4 Artificial Neural Network (ANN) Modeling

A feed-forward artificial neural network (ANN) with a multilayer perceptron (MLP) architecture was developed using JMP Pro 16 (SAS Institute Inc., Cary, NC, USA). The MLP consisted of an input layer with four neurons (reaction time, temperature, enzyme amount, and ultrasonic power), one hidden layer with ten neurons (H1–H10), and one output neuron representing the molar conversion of 2-PO (Fig. 1). A Gaussian activation function was applied, and network training was performed using the Gauss-Newton algorithm (Lai et al., 2017). Of the 27 CCRD experimental runs, 22 were used for model training and 5 for validation. Model performance was evaluated using the coefficient of determination (R^2), root mean square error (RMSE), and mean absolute deviation (MAD), as defined in Eqs. (2)–(4):

$$R^2 = 1 - \frac{\sum_{i=1}^{n} (Y_{pre} - Y_{exp})^2}{\sum_{i=1}^{n} (Y_m - Y_{exp})^2} \quad \ldots\ldots\ldots\ldots\ldots\ldots\ldots\ldots(2)$$

$$RMSE = \sqrt{\frac{\sum_{i=1}^{n} (Y_{pre} - Y_{exp})^2}{n}} \quad \ldots\ldots\ldots\ldots\ldots\ldots\ldots\ldots(3)$$

$$MAD = \left(\frac{\sum_{i=1}^{n} (|Y_{exp} - Y_{pre}| / Y_{pre})}{n} \right) \times 100 \quad \ldots\ldots\ldots\ldots\ldots\ldots\ldots(4)$$

where Y_{pre} is the predicted value, and Y_{exp} is the experimental value, Y_m is the mean

experimental molar conversion, and n is the sample size.

2.5 Analytical Methods

The molar conversion of 2-PO was determined by quantitative gas chromatography. A 1 μL aliquot of the reaction mixture was injected into an Agilent 7890A gas chromatograph (Agilent Technologies, Santa Clara, CA, USA) equipped with a flame ionization detector (FID) and an HP-5 capillary column (30 m × 0.32 mm i.d., 0.25 μm film thickness). The injector and detector temperatures were maintained at 230 °C and 250 °C, respectively. The oven temperature program was as follows: initial hold at 80°C for 2 min, ramp to 100 °C at 20 °C/min (held for 3 min), then ramp to 230 °C at 50 °C/min (held for 1.5 min). Nitrogen was used as the carrier gas at a flow rate of 3.5 mL/min. Calibration curves were constructed using pure 2-PE and C8 standards to correlate peak areas with molar concentrations. The molar conversion (%) was calculated as [mmol of 2-PO / (mmol of C8 + mmol of 2-PO)] × 100.

2.6 Molecular docking analysis

Molecular docking was performed to evaluate the binding interactions between *Candida antarctica* lipase B (CALB) and the substrates C8, 2-PE, and the ester product 2-phenylethyl octanoate (2-PO). The crystal structure of CALB was retrieved from the Protein Data Bank (PDB ID: 1TCB), and the three-dimensional structures of the ligands

were obtained from the PubChem database. Receptor preparation was performed using AutoDock Tools (v1.5.7), including removal of water molecules and co-crystallized ligands, followed by addition of polar hydrogens and assignment of Kollman charges. The docking grid box was centered on the catalytic triad (Ser105, His224, and Asp187) at coordinates (x = 13.081, y = 11.905, z = 30.814) with a box size of 18 × 18 × 18 Å. Docking calculations were carried out using AutoDock Vina (v1.2.7) with an exhaustiveness value of 32. The binding pose with the lowest binding energy and correct catalytic orientation was selected for further analysis.

Post-docking analysis and three-dimensional visualization were conducted using PyMOL (v2.5.2). To validate the catalytic mechanism, the protonation states of active site residues were manually corrected (HIE state for His224), and the proton relay network was visualized. Catalytic interactions were evaluated based on the heavy-atom distance (< 3.5 Å) between the nucleophilic oxygen of Ser105 and the carbonyl carbon of each ligand. Two-dimensional interaction diagrams were generated using BIOVIA Discovery Studio Visualizer (v21.1.0) to identify hydrogen bond and hydrophobic contact patterns.

2.7 Evaluation of Sustainability Metrics

The environmental impact of the solvent-free enzymatic synthesis of 2-PO was assessed using four established green chemistry metrics: E-factor, atom economy (AE), mass intensity (MI), and reaction mass efficiency (RME) (Constable et al., 2002; Sheldon,

187 2017). These metrics were calculated based on the masses of reactants and products
188 involved in the esterification reaction. In accordance with the method described by Sheldon
189 (Sheldon, 2017), water generated as a by-product of direct esterification was excluded from
190 the waste mass calculation, given that 2-PO was the sole target product. Furthermore, to
191 accurately reflect practical industrial downstream processing, a 90% substrate recovery of
192 the excess unreacted 2-PE was integrated into the system boundary for the calculation of
193 the net E-factor and MI (Sheldon, 2017). These metrics provide a quantitative basis for
194 evaluating the material efficiency of the developed process and for informing subsequent
195 scale-up evaluation.

196 **3. Results and Discussion**

197 **3.1 Molecular Docking Analysis of Substrate and Product Binding**

198 Molecular docking was used to examine the predicted binding interactions of C8, 2-
199 PE, and 2-PO with Candida antarctica lipase B (CALB), the catalytic component of
200 Novozym® 435. CALB contains the Ser105–His224–Asp187 catalytic triad (Uppenberg et
201 al., 1995), whereas Thr40 and Gln106 form the oxyanion hole involved in transition-state
202 stabilization (Zhang et al., 2022). The selected docking poses were evaluated based on their
203 binding energies and relative positions within the active-site region.

204 *Step 1: Hydrophobic Positioning of the Acyl Donor (C8) in the Active-Site Region*

205 C8 docked into the active site with a binding energy of −4.691 kcal/mol. The docked
206 octanoyl chain was positioned near Leu278, Ile189, Val154, and Ala281 in the CALB
207 active-site region (Fig. 2A–B); these residues are located in the hydrophobic region of the
208 catalytic cavity (Dettori et al., 2018). Trp104 forms part of the stereospecificity pocket and
209 is associated with the spatial recognition of alcohol substituents (Juhl et al., 2009;
210 Uppenberg et al., 1995). Its position at the active-site entrance (Fig. 2A) may constrain the
211 direction and angle of substrate access. The carbonyl oxygen of C8 was positioned 3.1 Å
212 from Thr40, whereas the Ser105–His224 and His224–Asp187 distances were 3.0 and 2.9
213 Å, respectively (Fig. 2B), suggesting a geometry potentially compatible with nucleophilic
214 acylation.

215 *Step 2: Putative Near-Attack Conformation (NAC) and Possible Conformational*
216 *Accommodation of the Active Site*

217 A modeled complex containing 2-PE and the Ser105–C8 acyl-enzyme intermediate
218 was examined to assess the positioning of the alcohol substrate relative to the acyl group
219 (Fig. 2C–D). Two structural features were considered: the Thr40–acyl oxygen distance and
220 the position of the 2-PE hydroxyl group.

221 (A) Possible Conformational Accommodation in the Oxyanion-Hole Region:

222 The Thr40–acyl oxygen distance increased from 3.1 Å in the Step 1 pose to 4.1 Å in

223 the Step 2 pose (Fig. 2D). This difference may reflect conformational accommodation in
224 the oxyanion-hole region. Backbone adjustments near Thr40 and Gly41 have been reported
225 to displace a backbone oxygen atom by up to 2.1 Å (Juhl et al., 2009). The distance
226 observed here may therefore be related to accommodation of the 2-PE aromatic group.

227 (B) Ethyl Linker Flexibility in Substrate Positioning:

228 Despite steric restriction imposed by Trp104, a nucleophilic O⋯C distance of 3.5 Å
229 was observed (Fig. 2C), consistent with a putative near-attack conformation (NAC) (Hur
230 & Bruice, 2003). Compared with rigid cinnamate-type substrates (Hao et al., 2024), the
231 saturated ethyl linker ($-CH_2CH_2-$) of 2-PE may provide sufficient flexibility for the
232 hydroxyl group to approach the acyl group while the aromatic ring remains anchored in the
233 hydrophobic environment. The modeled ternary complex exhibited a binding energy of
234 −4.799 kcal/mol, supporting the feasibility of this putative pre-reaction configuration.

235 *Step 3: Putative Thermodynamic Basis of Product Inhibition and Its Possible Link to*
236 *Reaction Kinetics*

237 The product 2-phenylethyl octanoate (2-PO) exhibited a predicted binding energy of
238 −6.524 kcal/mol, more negative than those of 2-PE (−5.039 kcal/mol), C8 (−4.691
239 kcal/mol), and the modeled Ser105–C8 acyl-enzyme intermediate (−4.799 kcal/mol). The
240 difference between the predicted docking scores (1.49–1.83 kcal/mol) may be related to the

241 kinetic plateau observed beyond 10 min in Section 3.2. The higher predicted binding
242 affinity of 2-PO may constitute a putative thermodynamic sink that competitively restricts
243 substrate access to the active site. As shown in Fig. 2F, 2-PO formed hydrogen bonds with
244 Ser105 and His224 at distances of 3.1 Å and 3.2 Å, respectively. His224 is the catalytic-
245 triad residue established to mediate proton transfer to the alcohol oxygen of the substrate
246 during acyl transfer (Uppenberg et al., 1995); the observed hydrogen bond with 2-PO may
247 therefore reflect occupancy of this catalytically relevant position by the product, rather than
248 proton transfer itself. The concurrent hydrogen bond with Ser105, the catalytic nucleophile,
249 further supports the interpretation that 2-PO occupies the catalytic pocket in a manner that
250 may restrict access of subsequently entering substrates. This trend is consistent with
251 previous reports that increasing acyl-chain length progressively enhances binding affinity
252 within the CALB active site (Bian et al., 2024). The stronger predicted binding of 2-PO
253 may also hinder product release. Together with the kinetic plateau observed in Section 3.2,
254 these docking results suggest that product-associated active-site occupancy may contribute
255 to the reduced reaction rate at later times; direct kinetic validation is required to test this
256 mechanism.

257 **3.2 Single-factor tests**

258 Fig. 3 illustrates the influence of reaction time (0–60 min) on the molar conversion of
259 2-PO under fixed conditions (55 °C, 150 W, and an enzyme amount of 1000 PLU). Catalytic

efficiency was high, with conversion reaching 82.4% within the first 10 min, representing approximately 94% of the maximum conversion (87.4%) attained at 60 min. Beyond 10 min, the reaction profile exhibited a distinct plateau, consistent with water accumulation-mediated equilibrium inhibition, a phenomenon frequently encountered in solvent-free enzymatic esterification (Foresti et al., 2007). The kinetic behaviour may also be interpreted in light of the docking analysis in Section 3.1, in which potential 2-PO occupancy of the CALB active site was identified as a possible structural contributor to the rapid attainment of the plateau.

The possible molecular basis for this rate-limiting behavior is reflected in the predicted binding affinities determined in Section 3.1: the product 2-PO (−6.524 kcal/mol) exhibited a more negative predicted binding energy than both the alcohol substrate 2-PE (−5.039 kcal/mol) and the acyl donor C8 (−4.691 kcal/mol), suggesting a putative thermodynamic trap that may competitively occupy the active site and retard subsequent substrate binding. The highly viscous, solvent-free mixture of 2-PE and C8 would conventionally impose substantial mass-transfer resistance; however, the rapid initial conversion observed here is consistent with ultrasonic cavitation disrupting the substrate matrix and diminishing interfacial resistance, in line with sonochemical acceleration reported in analogous high-viscosity biocatalytic systems (Tomke & Rathod, 2015; Tsai et al., 2022). To date, the only reported systematic optimization of 2-PO enzymatic synthesis employed Lipozyme® RM

IM in a hexane-based system, requiring up to 2 hours to achieve 80% conversion via transesterification with glyceryl trioctanoate under optimized conditions (Šinkūnienė et al., 2014). Notably, even under ultrasound irradiation, the solvent-free esterification of butyl caprylate, which shares the same C8 acyl donor and process conditions (Novozym® 435, solvent-free, ultrasonication) but lacks the additional steric burden of an aromatic alcohol, still required 3.5 hours to attain 95% conversion (Sose & Rathod, 2021), further underscoring the exceptional efficiency achieved in the present system despite the dual mass transfer and steric constraints imposed by 2-PE. The more than 6-fold reduction in reaction time achieved in the present system is consistent with the combined contribution of two distinct mechanisms: ultrasonic cavitation alleviating bulk-phase mass-transfer resistance in the solvent-free reaction medium, and acoustic energy potentially facilitating product release from the CALB active site, as inferred from the stronger predicted binding affinity of 2-PO observed in the docking analysis (Section 3.1). The docking results further indicate that product-associated active-site occupancy may contribute to the observed kinetic plateau, although the underlying inhibition mechanism requires direct kinetic validation. Consequently, a reaction time range of 2–10 min was selected for the subsequent central composite rotatable design (CCRD).

3.3 Optimization of 2-PO Synthesis by RSM and ANN

3.3.1 CCRD Experimental Design and RSM Model

A 5-level-4-factor central composite rotatable design (CCRD) was employed to evaluate the effects of reaction time (X_1), temperature (X_2), enzyme amount (X_3), and ultrasonic power (X_4) on the molar conversion of 2-PO. The 27 experimental runs yielded molar conversions ranging from 45.08% to 81.67% (Table 1). The second-order response surface model was derived as Eq. (5):

$$Y(\%) = -492.80 + 12.12\,X_1 + 5.54\,X_2 + 0.21\,X_3 + 3.80\,X_4 + 1.54\times10^{-3}\,X_1X_2 - 2.23\times10^{-3}\,X_1X_3 + 0.03\,X_1X_4 - 2.86\times10^{-4}\,X_2X_3 - 0.02\,X_2X_4 - 5.94\times10^{-4}\,X_3X_4 - 0.90\,X_1^2 - 0.02\,X_2^2 - 4.52\times10^{-5}\,X_3^2 - 7.66\times10^{-3}\,X_4^2 \quad (5)$$

ANOVA results (Table 2) confirmed model significance ($p = 0.0002$), with $R^2 = 0.9333$, indicating that the model explained 93.33% of the variation in molar conversion. Among the linear terms, enzyme amount (X_3) had the greatest influence on molar conversion ($F = 63.29$, $p < 0.0001$), followed by reaction time (X_1, $p = 0.0002$), temperature (X_2, $p = 0.0009$), and ultrasonic power (X_4, $p = 0.0090$). Among interaction terms, only X_2X_4 was significant ($p = 0.0065$). The quadratic terms X_1^2 ($p = 0.0055$) and X_3^2 ($p = 0.0206$) were also significant. However, the adjusted R^2 of 0.8484 and coefficient of variation (CV) of 6.42% indicated that the RSM model did not fully capture the nonlinear relationships among variables. ANN was therefore adopted to improve prediction accuracy.

3.3.2 Response Surface Analysis

316 The significant interaction between temperature and ultrasonic power (X_2X_4, $p = 0.0065$)
317 was examined using contour and three-dimensional surface plots (Fig. 4). The highest
318 molar conversion was obtained at approximately 55–65 °C combined with 120–135 W.
319 When both parameters were simultaneously elevated beyond these ranges, molar
320 conversion declined sharply. This is consistent with results reported for solvent-free
321 Novozym® 435-catalyzed esterification under ultrasound (Sose & Rathod, 2021), wherein
322 conversion decreased from 95.33% to 89.63% when temperature exceeded 60 °C due to
323 enzyme denaturation and reduced cavitation intensity, and excessive acoustic power (>90
324 W) independently induced conformational changes and deactivation of the immobilized
325 enzyme. Under combined high-temperature and high-power conditions, these two
326 deactivation mechanisms act simultaneously, exceeding the tolerance threshold of
327 Novozym® 435 under combined thermal and acoustic stress (Delgado-Povedano & De
328 Castro, 2015; Khan et al., 2015). These results indicate that maintaining temperature and
329 ultrasonic power within their respective optimal ranges is essential for preserving
330 Novozym® 435 activity in the solvent-free system.

331 *3.3.3 ANN Model Performance and Comparison with RSM*

332 To overcome the limitations of RSM in capturing nonlinear variable interactions, an
333 ANN model with a 4-10-1 multilayer perceptron (MLP) topology was constructed (Fig. 1).
334 As summarized in Table 3, the ANN model outperformed RSM across all statistical metrics:

335 R^2 = 0.9974 vs. 0.9333, RMSE = 0.5535 vs. 4.1984, and MAD = 0.0064 vs. 0.0337. The
336 ANN parity plot (y = 0.9954x + 0.3586, R^2 = 0.9974) showed closer agreement with
337 experimental values than RSM (y = 0.9341x + 4.5029, R^2 = 0.9333) (Fig. 5). As shown in
338 Table 1, over 70% of ANN-predicted values deviated by less than 0.5% from experimental
339 results, whereas RSM showed larger deviations in several runs (e.g., Run 2: 7.39%; Run
340 15: 4.72%). The larger RSM deviations are attributable to its inherently quadratic structure,
341 which cannot adequately resolve sharp nonlinear responses. In contrast, the MLP
342 architecture effectively captured this nonlinear response surface through nonlinear hidden-
343 layer transformations. These results are consistent with previous studies reporting ANN
344 superiority over RSM in modeling nonlinear enzymatic and biochemical processes (Desai
345 et al., 2008; Huang, Kuo, et al., 2017; Yu et al., 2019).

346 *3.3.4 ANN-Based Optimization and Experimental Validation*

347 The ANN model identified the optimal conditions for maximum molar conversion of 2-
348 PO as: reaction time 6.48 min, temperature 57.34 °C, enzyme amount 1216.87 PLU, and
349 ultrasonic power 124.98 W, with a desirability value of 0.9464 and a predicted molar
350 conversion of 88.16% (Table 4). Triplicate experiments under ANN-optimized conditions
351 yielded 87.01 ± 1.02% (CV = 1.17%). The experimental value showed no significant
352 deviation from the ANN prediction of 88.16% (*t*-test, p = 0.189), but differed significantly
353 from the RSM prediction of 82.57% (*t*-test, p = 0.017), confirming the superior predictive

accuracy of ANN. In comparison, a maximum conversion of 92.4% required 6 h under conventional conditions (Tan et al., 2011), and 80% conversion in 2 h was reported for a hexane-based transesterification system (Šinkūnienė et al., 2014). The present system achieved 87.01% conversion in under 10 min without organic solvent, representing a greater than 10-fold reduction in reaction time, consistent with the principles of green chemistry (Anastas & Warner, 2000). Under the ANN-optimized conditions, a control reaction was performed using the same ultrasonic bath system with temperature maintained at 57.34 °C but with the ultrasonic function switched off, achieving 45.84% ± 2.66% molar conversion (CV = 5.80%, n = 3). In contrast, the reaction conducted with ultrasonic irradiation under identical conditions reached 87.01% ± 1.02% within 6.48 min. The higher conversion obtained in the presence of ultrasound could be associated with improved mixing and substrate transport in the solvent-free reaction medium.

3.4 Biocatalyst Reusability and Operational Stability

The reusability of immobilized Novozym® 435 was evaluated over 10 consecutive reaction cycles in the ultrasound-assisted solvent-free system, with the molar conversion of 2-PO measured at the end of each cycle. The conversion of the first cycle was defined as 100%, and subsequent values were expressed as relative molar conversions (Fig. 6). The immobilized biocatalyst exhibited remarkable operational stability, maintaining a relative conversion of over 94.0% throughout the first eight cycles. By the end of the 10th cycle,

373 the enzyme still retained 88.8% of its initial activity, indicating a gradual decline in catalytic
374 performance. This activity decline, consistent with the enzyme inactivation phenomena
375 reported in similar ultrasonication-assisted systems using C8 (Kuo et al., 2025), may be
376 attributed to partial enzyme denaturation caused by the localized acidic microenvironment
377 generated by unreacted C8 at the enzyme–water interface, as well as enzyme leaching from
378 the macroporous acrylic resin support over repeated cycles. Given the high recyclability
379 and ease of biocatalyst recovery by size-based separation, these results suggest that
380 immobilized Novozym® 435 under the optimized conditions is highly suitable for repeated
381 use in scaled-up 2-PO biosynthesis.

382 **3.5 Sustainability Metrics Evaluation**

383 The sustainability metrics of the ultrasound-assisted solvent-free process for 2-PO
384 synthesis are summarized in Table 5. The process achieved an atom economy of 93.24%
385 and an E-factor of 0.49 kg/kg, substantially lower than those reported for hexyl hexanoate
386 (14.77 kg/kg) and cinnamyl butyrate (4.76 kg/kg) under solvent-free conditions (Dudu et
387 al., 2021; Dudu et al., 2024). This low E-factor is primarily attributed to the 90% substrate
388 recovery strategy integrated into the process design (Sheldon, 2017). The mass intensity
389 (MI) of 1.49 kg/kg approaches the theoretical minimum of 1.00 kg/kg and significantly
390 outperforms both hexyl hexanoate (16.07 kg/kg) and the aqueous production of cinnamyl
391 acetate (35.48 kg/kg) (Dudu et al., 2021; Perdomo et al., 2019). The favorable performance

of these metrics is primarily attributable to the 90% substrate recovery strategy and the elimination of auxiliary solvents in the solvent-free system, which together minimized waste generation and maximized mass utilization (Trost, 1991). These material efficiency gains are complementary to the process advantages discussed in Sections 3.1 and 3.2, wherein ultrasonic cavitation may have enhanced mixing and mass transfer, contributing to the short reaction time achieved without additional resource input.

4. Conclusion

In this study, an ultrasound-intensified solvent-free biocatalytic process was developed for the synthesis of 2-phenethyl octanoate (2-PO) using immobilized Novozym® 435. Process conditions were optimized by integrating response surface methodology and artificial neural networks, achieving 87.01 ± 1.02% molar conversion within 6.48 min under ultrasound, substantially higher than the non-ultrasonicated control. Molecular docking suggested that C8 and 2-PE could be accommodated within the Ser105-His224-Asp187 catalytic triad in catalytically relevant conformations, while the stronger predicted binding affinity of 2-PO relative to the substrates may contribute to product-associated active-site occupancy and the kinetic plateau observed in later reaction stages. The process exhibited favorable sustainability metrics (E-factor of 0.49 kg/kg, atom economy of 93.24%) and retained 88.8% relative molar conversion after 10 consecutive cycles,

indicating operational stability. These findings support solvent-free direct esterification, intensified by ultrasound, as a scalable biocatalytic route for producing 2-PO as a natural flavor ester within food bioprocessing applications.

Author contributions

Ming-Fang Tsai: Conceptualization, Methodology, Investigation, Formal analysis, Visualization, Writing – original draft; Shuo-Wen Tsai: Conceptualization, Supervision, Writing – review & editing; Chwen-Jen Shieh: Conceptualization, Supervision, Writing – review & editing.

Funding

No funding was received to assist with the preparation of this manuscript.

Competing Interests

The authors have no relevant financial or non-financial interests to disclose.

Data availability

The data supporting this article, including experimental results, green chemistry metrics, molecular docking outputs, RSM and ANN modelling data, and enzyme reusability results, are included as part of the manuscript.

References

Anastas, P. T., & Warner, J. C. (2000). *Green chemistry: theory and practice*. Oxford university press.

Bernardino, A. R., Torres, C. A., Crespo, J. G., & Reis, M. A. (2024). Biotechnological 2-phenylethanol production: recent developments. *Molecules*, *29*(23), 5761.

Bian, Y., Zhang, Y., Wang, T., Yang, C., Feng, Z., Goh, K. L., Zhou, Y., & Zheng, M. (2024). Insights into the enzymatic synthesis of alcoholic flavor esters with molecular docking analysis. *LWT - Food Science and Technology*, *200*, 116206.

Camciuc, M., Bessière, J. M., Vilarem, G., & Gaset, A. (1998). Volatile components in okra seed coat. *Phytochemistry*, *48*(2), 311–315.

Cha, H.-J., Park, J.-B., & Park, S. (2019). Esterification of secondary alcohols and multi-hydroxyl compounds by Candida antarctica lipase B and subtilisin. *Biotechnology and Bioprocess Engineering*, *24*(1), 41–47.

Chaibakhsh, N., Basri, M., Anuar, S. H. M., Rahman, M. B. A., & Rezayee, M. (2012). Optimization of enzymatic synthesis of eugenol ester using statistical approaches. *Biocatalysis and Agricultural Biotechnology*, *1*(3), 226–231.

Constable, D. J., Curzons, A. D., & Cunningham, V. L. (2002). Metrics to 'green'chemistry—which are the best? *Green Chemistry*, *4*(6), 521–527.

Delgado-Povedano, M., & De Castro, M. L. (2015). A review on enzyme and ultrasound: A controversial but fruitful relationship. *Analytica chimica acta*, *889*, 1–21.

Desai, K. M., Survase, S. A., Saudagar, P. S., Lele, S., & Singhal, R. S. (2008). Comparison of artificial neural network (ANN) and response surface methodology (RSM) in fermentation media optimization: case study of fermentative production of scleroglucan. *Biochemical Engineering Journal*, *41*(3), 266–273.

Dettori, L., Jelsch, C., Guiavarc'h, Y., Delaunay, S., Framboisier, X., Chevalot, I., & Humeau, C. (2018). Molecular rules for selectivity in lipase-catalysed acylation of lysine. *Process biochemistry*, *74*, 50–60.

Dudu, A. I., Lăcătuş, M. A., Bencze, L. C., Paizs, C., & Toşa, M. I. (2021). Green process for the enzymatic synthesis of aroma compounds mediated by lipases entrapped in tailored sol–gel matrices. *ACS Sustainable Chemistry & Engineering*, *9*(15), 5461–5469.

Dudu, A. I., Paizs, C., & Toşa, M. I. (2024). Optimization of reaction parameters for the synthesis of natural aroma esters by factorial design. *Reaction Chemistry & Engineering*, *9*(11), 2994–3002.

Foresti, M. L., Pedernera, M., Bucalá, V., & Ferreira, M. L. (2007). Multiple effects of water on solvent-free enzymatic esterifications. *Enzyme and Microbial Technology*, *41*(1-2), 62–70.

Gandhi, N. N., & Mukherjee, K. D. (2001). Specificity of papaya lipase in esterification of aliphatic alcohols a comparison with microbial lipases. *Journal of the American Oil Chemists' Society*, *78*(2), 161–165.

Hao, L., Zou, Y., Li, X., Xin, X., Zhang, M., & Zhao, G. (2024). Green biocatalytic synthesis of (hydroxy)cinnamic monoterpenyl esters in biomass solvent: Mechanism underlying different reaction efficiency. *Food Bioscience*, *61*, 104914.

Horchani, H., Salem, N. B., Zarai, Z., Sayari, A., Gargouri, Y., & Chaâbouni, M. (2010). Enzymatic synthesis of eugenol benzoate by immobilized Staphylococcus aureus lipase: Optimization using response surface methodology and determination of antioxidant activity. *Bioresource Technology*, *101*(8), 2809–2817.

Huang, S.-M., Kuo, C.-H., Chen, C.-A., Liu, Y.-C., & Shieh, C.-J. (2017). RSM and ANN modeling-based optimization approach for the development of ultrasound-assisted liposome encapsulation of piceid. *Ultrasonics Sonochemistry*, *36*, 112–122.

Huang, S.-M., Li, H.-J., Liu, Y.-C., Kuo, C.-H., & Shieh, C.-J. (2017). An efficient approach for lipase-catalyzed synthesis of retinyl laurate nutraceutical by combining ultrasound assistance and artificial neural network optimization. *Molecules*, *22*(11), 1972.

Hur, S., & Bruice, T. C. (2003). The near attack conformation approach to the study of the chorismate to prephenate reaction. *Proceedings of the National Academy of Sciences*, *100*(21), 12015–12020.

Joint FAO/WHO Expert Committee on Food Additives. (2002). *Evaluation of certain food additives and contaminants: Fifty-ninth report of the Joint FAO/WHO Expert Committee on Food Additives* (913). (WHO Technical Report Series, Issue.

Juhl, P. B., Trodler, P., Tyagi, S., & Pleiss, J. (2009). Modelling substrate specificity and enantioselectivity for lipases and esterases by substrate-imprinted docking. *BMC Structural Biology*, *9*(1), 39.

Khan, N. R., Jadhav, S. V., & Rathod, V. K. (2015). Lipase catalysed synthesis of cetyl oleate using ultrasound: optimisation and kinetic studies. *Ultrasonics Sonochemistry*, *27*, 522–529.

Kuo, C.-H., Hsiao, F.-W., Chen, J.-H., Hsieh, C.-W., Liu, Y.-C., & Shieh, C.-J. (2013). Kinetic aspects of ultrasound-accelerated lipase catalyzed acetylation and optimal synthesis of 4′-acetoxyresveratrol. *Ultrasonics Sonochemistry*, *20*(1), 546–552.

Kuo, C.-H., Nargotra, P., Lin, T.-H., Shieh, C.-J., & Liu, Y.-C. (2025). Ultrasonication-assisted lipase-catalyzed esterification of chlorogenic acid: A comparative study using fatty alcohol and acids in solvent and solvent-free conditions. *Ultrasonics Sonochemistry*, *113*, 107218.

Lai, W. H., Kek, S. L., & Tay, K. G. (2017). Solving nonlinear least squares problem using Gauss-Newton method. *International Journal of Innovative Science, Engineering*

& Technology, *4*(1), 258–262.

Lipshutz, B. H., & Handa, S. (2026). Modernizing the 12 principles of green chemistry: it's time. *Green Chemistry*.

Mat Radzi, S., Hanif, M. Z. R., & Syamsul, K. M. W. (2016). Optimization of eugenol ester using statistical approach of response surface methodology. *Materials Science Forum*, *857*, 469–474.

Nieto, S., Villa, R., Donaire, A., & Lozano, P. (2021). Ultrasound-assisted enzymatic synthesis of xylitol fatty acid esters in solvent-free conditions. *Ultrasonics Sonochemistry*, *75*, 105606.

Perdomo, I. C., Gianolio, S., Pinto, A., Romano, D., Contente, M. L., Paradisi, F., & Molinari, F. (2019). Efficient enzymatic preparation of flavor esters in water. *Journal of agricultural and food chemistry*, *67*(23), 6517–6522.

Sheldon, R. A. (2017). The E factor 25 years on: the rise of green chemistry and sustainability. *Green Chemistry*, *19*(1), 18–43.

Šinkūnienė, D., Kazlauskas, S., & Bendikienė, V. (2014). Enzymatic phenethyl octanoate synthesis: lipase selection and reaction optimization by response surface methodology. *chemija*, *25*(3), 185–194.

Sose, M. T., & Rathod, V. K. (2021). Ultrasound assisted enzyme catalysed synthesis of butyl caprylate in solvent free system. *Indian Chemical Engineer*, *63*(4), 402–413.

Sousa, H. R., Manoel, E. A., & Ferreira-Leitão, V. S. (2020). Kinetic study on the enzymatic esterification of octanoic acid and n-octanol by immobilized Candida antarctica lipase B. *Biocatalysis and Biotransformation*, *38*(5), 329–340.

Sousa, R. R., Silva, A. S. A., Fernandez-Lafuente, R., & Ferreira-Leitão, V. S. (2021). Solvent-free esterifications mediated by immobilized lipases: a review from thermodynamic and kinetic perspectives. *Catalysis Science & Technology*, *11*(17), 5696–5711.

Suarez-Escobedo, L., & Gotor-Fernandez, V. (2021). Solvent role in the lipase-catalysed esterification of cinnamic acid and derivatives. Optimisation of the biotransformation conditions. *Tetrahedron*, *81*, 131873.

Tan, H. S. G., Yu, B., Curran, P., & Liu, S. Q. (2011). Lipase-catalysed synthesis of natural aroma-active 2-phenylethyl esters in coconut cream. *Food chemistry*, *124*(1), 80–84.

Tomke, P. D., & Rathod, V. K. (2015). Ultrasound assisted lipase catalyzed synthesis of cinnamyl acetate via transesterification reaction in a solvent free medium. *Ultrasonics Sonochemistry*, *27*, 241–246.

Trost, B. M. (1991). The atom economy—a search for synthetic efficiency. *Science*, *254*(5037), 1471–1477.

Tsai, M. F., Huang, S. M., Huang, H. Y., Tsai, S. W., Kuo, C. H., & Shieh, C. J. (2022).

Ultrasound plus vacuum-system-assisted biocatalytic synthesis of octyl cinnamate and response surface methodology optimization. *Molecules*, *27*(21), 7148.

Uppenberg, J., Oehrner, N., Norin, M., Hult, K., Kleywegt, G. J., Patkar, S., & Jones, T. A. (1995). Crystallographic and molecular-modeling studies of lipase B from Candida antarctica reveal a stereospecificity pocket for secondary alcohols. *Biochemistry*, *34*(51), 16838–16851.

Xu, C., Zhang, H., Shi, J., Zheng, M., Xiang, X., Huang, F., & Xiao, J. (2018). Ultrasound irradiation promoted enzymatic alcoholysis for synthesis of monoglyceryl phenolic acids in a solvent-free system. *Ultrasonics Sonochemistry*, *41*, 120–126.

Yu, H.-C., Huang, S.-M., Lin, W.-M., Kuo, C.-H., & Shieh, C.-J. (2019). Comparison of artificial neural networks and response surface methodology towards an efficient ultrasound-assisted extraction of chlorogenic acid from Lonicera japonica. *Molecules*, *24*(12), 2304.

Zhang, T., Zhang, Y., Deng, C., Zhong, H., Gu, T., Goh, K. L., Han, Z., Zheng, M., & Zhou, Y. (2022). Green and efficient synthesis of highly liposoluble and antioxidant L-ascorbyl esters by immobilized lipases. *Journal of Cleaner Production*, *379*, 134772.

Table 1. Central composite rotatable design (CCRD) matrix showing coded factor levels, experimental 2-PO molar conversions, and corresponding RSM- and ANN-predicted values for the 27 experimental runs.

Independent Variables	Unit	Symbols	Coded Values				
			-2	-1	0	+1	+2
Reaction time	min	X_1	2	4	6	8	10
Temperature	°C	X_2	35	45	55	65	75
Enzyme amount	PLU	X_3	500	750	1000	1250	1500
Ultrasonic power	W	X_4	90	105	120	135	150

Run	Independent Variables [a]				2- Phenethyl Octanoate Molar Conversion (%)				
	X_1	X_2	X_3	X_4	Experimental Data	RSM-Predicted	RSM Deviation	ANN-Predicted	ANN Deviation
1	4	45	750	105	45.08	41.68	3.40	45.07	0.01
2	8	45	750	105	44.52	51.91	7.39	46.32	1.80
3	4	65	750	105	54.41	58.38	3.96	54.73	0.32
4	8	65	750	105	71.53	68.73	2.80	71.40	0.13
5	4	45	1250	105	61.16	64.00	2.84	61.37	0.22
6	8	45	1250	105	71.19	69.77	1.42	70.90	0.28
7	4	65	1250	105	77.26	77.83	0.57	77.25	0.01
8	8	65	1250	105	79.12	83.72	4.60	78.82	0.30
9	4	45	750	135	59.40	57.48	1.92	59.77	0.37
10	8	45	750	135	72.56	70.97	1.59	72.38	0.18
11	4	65	750	135	59.12	59.52	0.40	58.98	0.14
12	8	65	750	135	73.31	73.14	0.17	73.28	0.03
13	4	45	1250	135	69.10	70.88	1.78	69.25	0.15
14	8	45	1250	135	81.21	79.92	1.29	80.99	0.22
15	4	65	1250	135	74.78	70.07	4.72	74.25	0.53
16	8	65	1250	135	76.84	79.22	2.38	77.26	0.42
17	2	55	1000	120	52.05	53.12	1.07	51.31	0.74
18	10	55	1000	120	75.23	72.51	2.72	75.48	0.25
19	6	35	1000	120	62.59	62.23	0.37	61.65	0.95
20	6	75	1000	120	79.51	78.22	1.28	80.18	0.67
21	6	55	500	120	51.83	51.72	0.11	51.39	0.44
22	6	55	1500	120	81.67	80.13	1.55	82.23	0.55
23	6	55	1000	90	69.73	64.69	5.04	69.53	0.20
24	6	55	1000	150	72.60	75.99	3.39	72.86	0.26
25	6	55	1000	120	76.97	76.79	0.18	76.91	0.05
26	6	55	1000	120	77.50	76.79	0.72	76.91	0.59
27	6	55	1000	120	75.89	76.79	0.90	76.91	1.02

[a] Independent variable X_1: Reaction time (min), X_2: Temperature (°C), X_3: Enzyme amount (PLU), X_4: Ultrasonic power (W).

Table 2. Analysis of variance (ANOVA) for the RSM second-order polynomial model of 2-PO molar conversion.

Source	Sum of Squares	DF	Mean Square	F Value	*p*-Value Prob>F
Model	2943.01	14	210.22	10.99	0.0002 *
X_1	563.86	1	563.86	29.49	0.0002 *
X_2	383.97	1	383.97	20.08	0.0009 *
X_3	1209.99	1	1209.99	63.29	< 0.0001 *
X_4	191.48	1	191.48	10.01	0.0090 *
X_1X_2	0.015	1	0.015	0.0009	0.9781
X_1X_3	19.91	1	19.91	1.04	0.3294
X_1X_4	10.69	1	10.69	0.56	0.4703
X_2X_3	8.20	1	8.20	0.43	0.5260
X_2X_4	214.68	1	214.68	11.23	0.0065 *
X_3X_4	79.37	1	79.37	4.15	0.0664
X_1^2	226.83	1	226.83	11.86	0.0055 *
X_2^2	53.62	1	53.62	2.80	0.1222
X_3^2	139.55	1	139.55	7.30	0.0206 *
X_4^2	51.89	1	51.89	2.71	0.1277
Residual	210.31	11	19.12		
Lack of Fit	210.17	10	21.02	145.24	0.0645
Pure Error	0.14	1	0.14		
Cor Total	3153.32	25			
Std. Dev.	4.37	R-Squared	0.9333		
Mean	68.09	Adj R-Squared	0.8484		
CV%	6.42				
PRESS	1211.14				

Independent variable X_1: Reaction time (min), X_2: Temperature (°C), X_3: Enzyme amount (PLU), X_4: Ultrasonic power (W). * significant at *p*-value less than 0.05.

Table 3. Comparative predictive performance of RSM and ANN models for 2-PO molar conversion based on R^2, RMSE, and MAD.

Parameter	RSM	ANN
R^2	0.9333	0.9974
RMSE	4.1984	0.5535
MAD	0.0337	0.0064

Abbreviations: MAD, mean absolute deviation (%); RMSE, root mean square error; R^2, coefficient of determination.

Table 4. Estimated optimal reaction conditions for maximum 2-PO molar conversion predicted by the ANN model with corresponding desirability value.

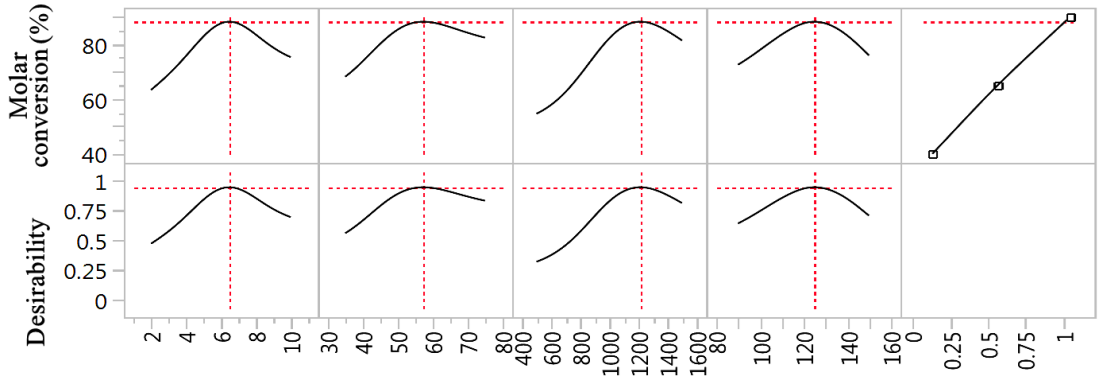

Parameters	Reaction time (min)	Temperature (°C)	Enzyme amount (PLU)	Ultrasonic power (W)	Desirability	Molar conversion (%)
Optimal prediction	6.48	57.34	1216.87	124.98	0.9464	88.16

Table 5. Sustainability metrics for the enzymatic synthesis of 2-PO compared to those for other aroma esters reported in the literature.

Sustainability metric	2-PO[a]	Cinnamyl butyrate[b]	Hexyl hexanoate[c]	Cinnamyl acetate[d]
E-factor	0.49	4.76	14.77	48.07
Atom economy (AE)	93.24	89.00	91.76	79.27
Mass intensity (MI)	1.49	6.04	16.07	35.48
Reaction mass efficiency (RME)	21.55	44.78	58.84	34.17

[a] Enzymatic esterification of octanoic acid (C8) with 2-phenylethanol in a solvent-free system (SFS) with 90% substrate recovery.

[b] Enzymatic esterification of butyric acid with cinnamyl alcohol in an SFS.

[c] Enzymatic esterification of hexanoic acid with hexan-1-ol in an SFS.

[d] Enzymatic transesterification of cinnamyl alcohol with ethyl acetate in phosphate buffer.

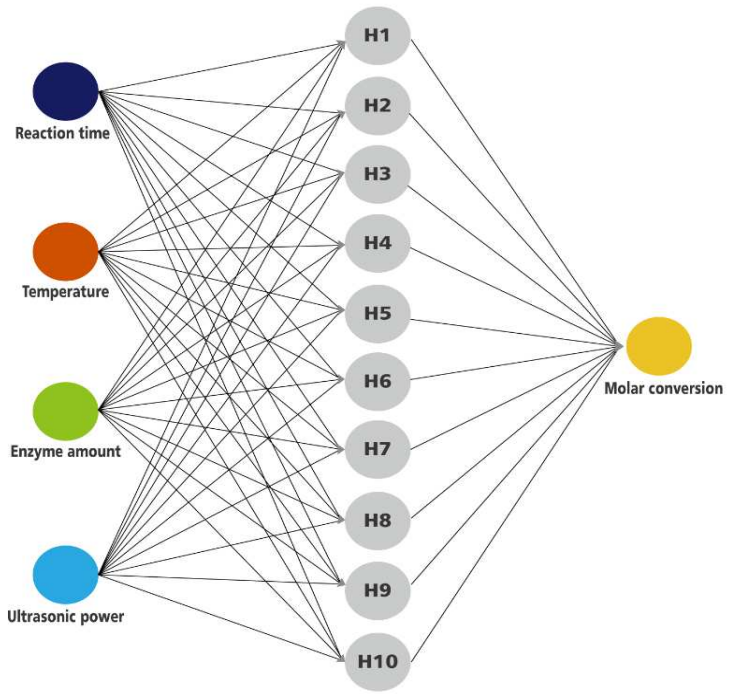

Fig. 1. Architecture of the multilayer perceptron (MLP) artificial neural network (ANN) model used for predicting 2-phenylethyl octanoate (2-PO) molar conversion, consisting of an input layer (4 neurons), one hidden layer (10 neurons, H1–H10), and one output neuron.

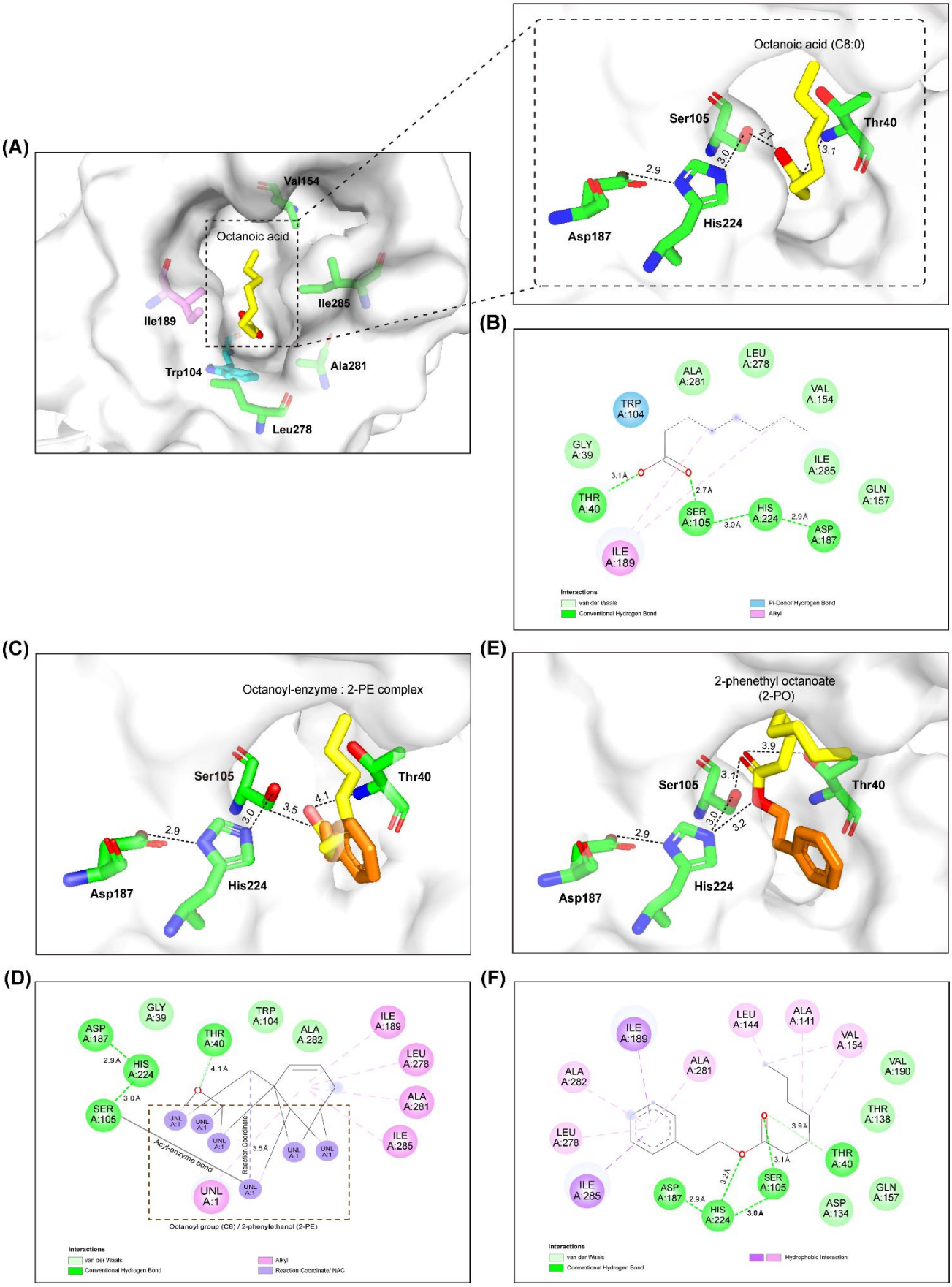

Fig. 2. Molecular docking analysis of predicted binding interactions relevant to CALB-catalyzed esterification of 2-phenylethanol (2-PE) with octanoic acid (C8). **(A, B)** Step 1: Predicted C8 binding pose in the hydrophobic active-site region, with Trp104 at the entrance to the stereospecificity pocket. **(C, D)** Step 2: Putative near-attack conformation (NAC) of 2-PE in the modeled Ser105–C8 acyl-enzyme complex, with a

3.5 Å nucleophilic O···C distance and an increase in the Thr40–acyl oxygen distance from 3.1 to 4.1 Å. **(E, F)** Step 3: Putative product inhibition by 2-phenylethyl octanoate (2-PO), suggested by its predicted occupancy of the CALB active site and hydrogen bonds with Ser105 and His224 at 3.1 and 3.2 Å, respectively.

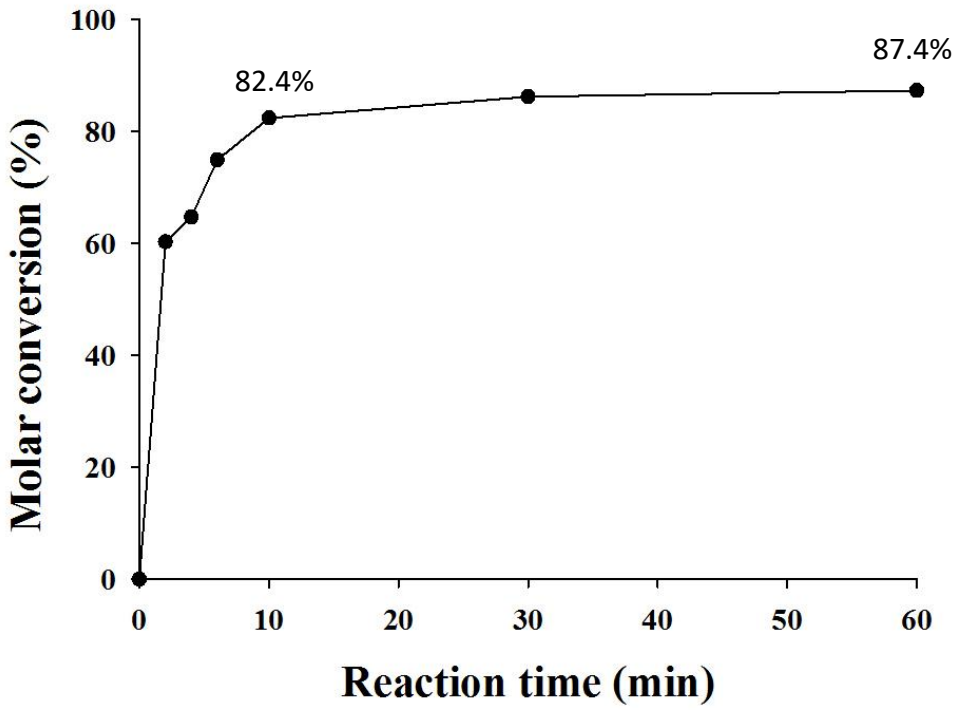

Fig. 3. Effect of reaction time on the molar conversion of 2-PO in the ultrasound-assisted solvent-free system. Conditions: 55 °C, 150 W, 1000 PLU Novozym® 435.

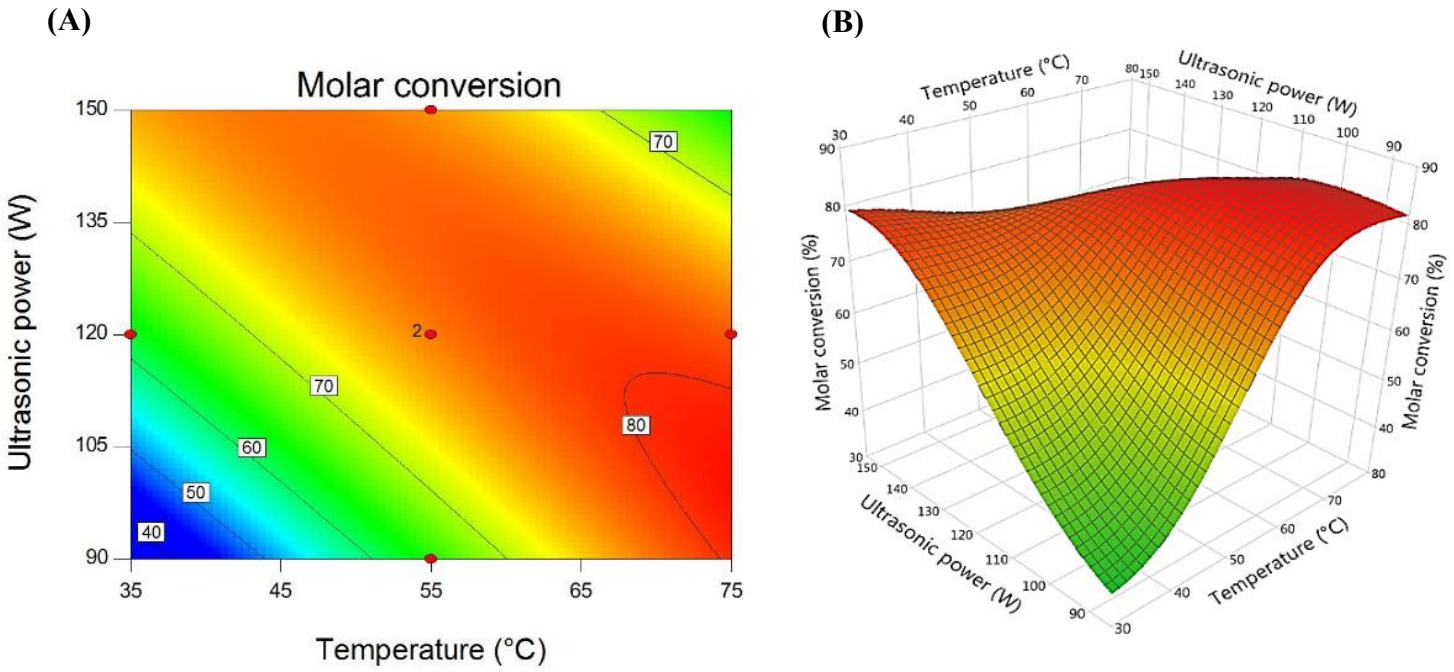

Fig. 4. Response surface plots showing the effect of temperature (°C) and ultrasonic power (W) on the molar conversion (%) of 2-phenylethyl octanoate (2-PO) synthesis catalyzed by CALB in a solvent-free system: (A) contour plot and (B) three-dimensional surface plot.

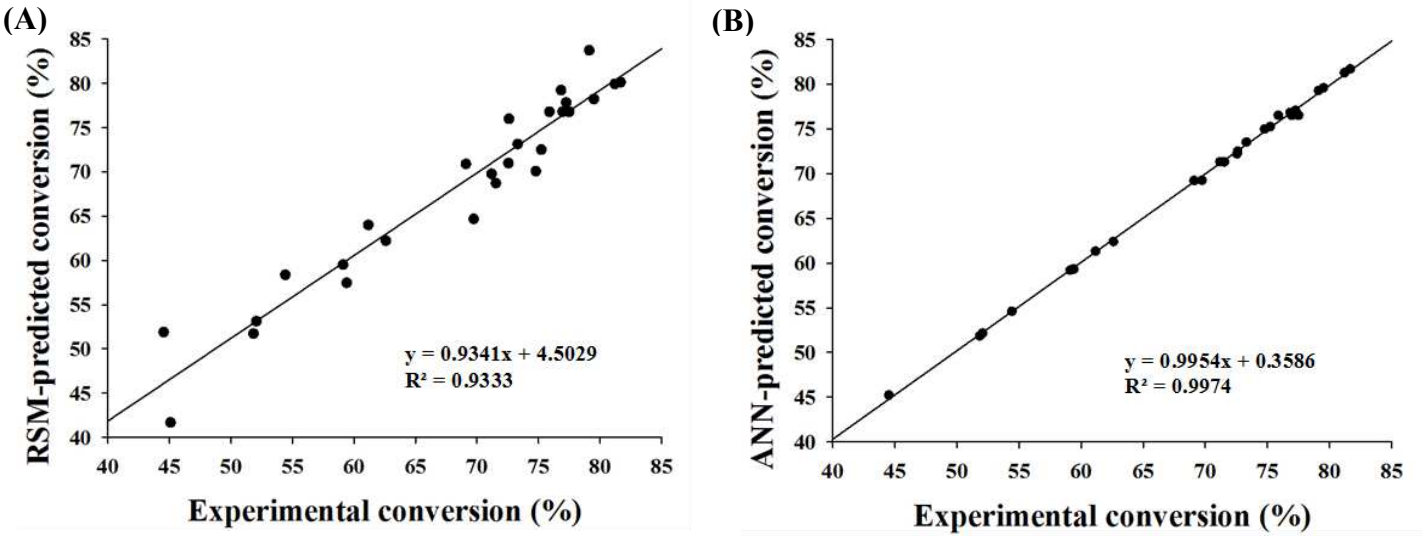

Fig. 5. Correlation between experimental and predicted molar conversion (%) for the optimization models: (A) RSM model ($y = 0.9341x + 4.5029$, $R^2 = 0.9333$) and (B) ANN model ($y = 0.9954x + 0.3586$, $R^2 = 0.9974$).

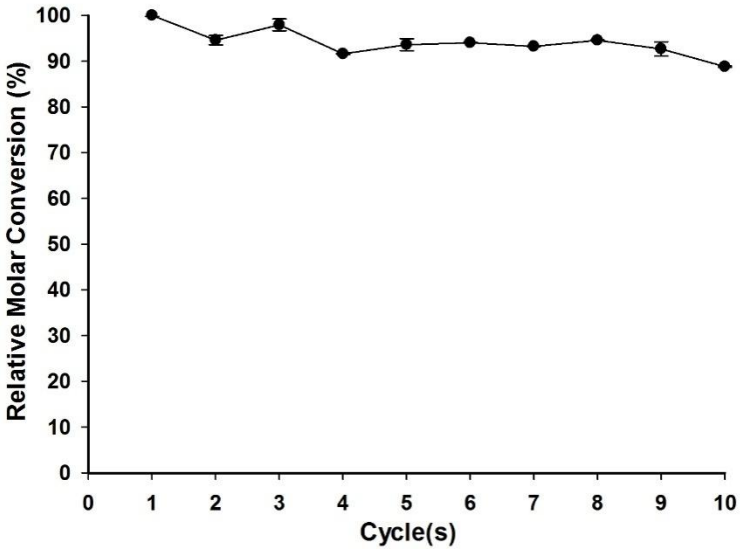

Fig. 6. Relative molar conversion of 2-PO over 10 consecutive reusability cycles of immobilized Novozym® 435. The molar conversion obtained in the first cycle was designated as 100%. Data are expressed as mean ± SD.